Journal of Volcanology and Geothermal Research 269 (2014) 1–13

Contents lists available at ScienceDirect

Journal of Volcanology and Geothermal Research

journal homepage: www.elsevier.com/locate/jvolgeores

A retrospective analysis of the Shinmoedake (Japan) eruption of 26–27 January 2011 by means of Japanese geostationary satellite data

F. Marchese [a,*], A. Falconieri [b], N. Pergola [a], V. Tramutoli [a,b]

[a] Institute of Methodologies for Environmental Analysis (IMAA), National Research Council (CNR), Tito Scalo (PZ), Italy
[b] School of Engineering, University of Basilicata, Potenza, Italy

ARTICLE INFO

Article history:
Received 10 July 2013
Accepted 29 October 2013
Available online 12 November 2013

Keywords:
Shinmoedake
Volcanic ash
Plume height
MTSAT
RST

ABSTRACT

During the sub-plinian eruptions of Mt. Shinmoedake (Japan) on 26–27 January 2011 a significant amount of ash was emitted into the atmosphere, destroying thousands of hectares of farm land, causing air traffic disruption, and forcing the closure of four railroad lines located around the volcano. In this work, a retrospective analysis of these eruptive events is presented, exploiting the high temporal resolution of the Japanese Multi-functional Transport Satellites (MTSAT) data to study thermal volcanic activity, to identify and track volcanic ash, and to determine the cloud-top height, inferring information about eruption features and space-time evolution. We show that a strong and sudden increase in the thermal signal occurred at Mt. Shinmoedake as a consequence of above mentioned eruptive events, generating hot spots timely detected by the RST_{VOLC} algorithm for the first time implemented here on data provided by geostationary satellites. This study also shows that the emitted ash plume, identified by means of the RST_{ASH} algorithm, strongly fluctuated in altitude, reaching a maximum height around 7.4 km above sea level, in agreement with information provided by the Tokyo VAAC. The plume heights derived in this work, by implementing the widely accepted cloud-top temperature method, appear also compatible with the values provided by independent weather radar measurements, with the main differences characterizing the third sub-plinian event that occurred in the afternoon of 27 January. The estimates of discharge rate, the temporal trend of ash affected areas, and the results of thermal monitoring reported in this work seem to indicate that the third sub-plinian event was the least intense. In spite of some limitations, this study confirms the potential of Japanese geostationary satellites in effectively monitoring volcanoes located in the West Pacific region, providing continuous information also about such critical parameters of ash clouds as the plume height. Such information is useful not only for driving numerical models, forecasting ash dispersion into the atmosphere, but also for characterizing eruption features and dynamics.

1. Introduction

Large amounts of ash can be injected into the atmosphere during major explosive eruptions posing a serious threat for population, environment, climate, and aviation safety (Tupper et al., 2009).

Satellite remote sensing thanks to the global coverage, to the continuity of observations and to multispectral data provided at different spatial and temporal resolutions represents an important tool for monitoring this phenomenon in a timely and effective way.

Considering that only about 50% of volcanoes are currently monitored by ground-based systems, which are generally not capable of providing large-scale measurements of volcanic phenomena, satellite sensors often represent the only instruments capable of providing information about ash clouds in the remote areas lying under major intercontinental air routes (International Civil Aviation Organization, 2007). Volcanic ash, being capable of damaging aircraft engines and affecting also other sensitive parts of airplanes (e.g. electrical and avionic units, fuel and hydraulic systems), represents a cause of important air traffic disruptions. As an example, during the Eyjafjallajökull (Iceland) eruptions of April–May 2010 several flights were canceled for safety issues, thousands of people were stranded at airports, and billions of dollars were lost by air companies. These eruptions encouraged a more extensive usage of data provided by sensors like SEVIRI (Spinning Enhanced Visible and Infrared Imager) for the early detection and the continuous monitoring of explosive eruptions, and for increasing capabilities in characterizing ash clouds operationally (ESA-EUMETSAT, 2010).

In this work, a retrospective analysis of Mt. Shinmoedake (Kyushu, Japan) eruption occurred on 26–27 January 2011, is presented. During this eruptive event, which began in the afternoon of 26 January at 14:50 LT (Local Time, LT = GMT + 9), a significant amount of tephra was injected into the atmosphere, causing the evacuation of the areas surrounding the volcano and the disruption of airplane and train services (Furukawa et al., 2011; Hashimoto et al., 2012). This eruption is analyzed here by means of infrared MTSAT (Multifunctional Transport Satellites) data, assessing the potential of Japanese geostationary satellites in timely detecting eruption onsets, in correctly identifying and

* Corresponding author. Tel.: +39 0971427225.
E-mail address: francesco.marchese@imaa.cnr.it (F. Marchese).

0377-0273/$ – see front matter © 2013 Elsevier B.V. All rights reserved.
http://dx.doi.org/10.1016/j.jvolgeores.2013.10.011

tracking ash clouds, and in providing accurate and useful information about eruption features and dynamics.

Two configurations of Robust Satellite Techniques (RST) multi-temporal approach (Tramutoli, 1998, 2007), the known cloud-top temperature method (Kienle and Shaw, 1979; Sawada, 1987; Glaze et al., 1989), and an empirical formulation largely used in literature for estimating the discharge rate from the cloud-top height (Sparks et al., 1997), are implemented in this work.

2. Mt. Shinmoedake eruptive events

The Mt. Shinmoedake (Fig. 1) is part of the Kirishima volcanic cluster which includes a series of small andesitic stratovolcanoes and two calderas (Imura and Kobayashi, 2001).

The largest eruptive event of Mt. Shinmoedake occurred during 1716–1717, when eruptive pumice-fall deposits, pyroclastic flows and mudflows were produced (Furukawa et al., 2011; Earthquake Research Institute, ERI, Univ.Tokyo, 2013; Earthquake Research Institute, University of Tokyo, 2013; Kato et al., 2013; Miyabuchi et al., 2013).

After this event, another phreatic eruption took place on 17 February 1959, with the ash deposits covering the towns of Takaharucho and Kobayashi, damaging forests and farmlands (Mizota and Faure, 1998; Japan Meteorological Agency, 2005).

In more recent years, small amounts of ash were emitted during November 1991–February 1992, after an intense seismic activity (Earthquake Research Institute, ERI, Univ.Tokyo, 2013; Earthquake Research Institute, University of Tokyo, 2013). A phreatic eruption occurred on 22 August 2008, when about 0.2 million tons of tephra were produced, and minor eruptions took place during March–July 2010 (Geshi et al., 2011; Kato et al., 2013).

The eruptive activity of this volcano in 2011 began on 19 January, when a small phreatomagmatic eruption occurred generating an ash cloud that drifted towards the SE. On 22 January another ash plume was emitted reaching an altitude of 1.8–2.1 km above sea level (asl) (Miyabuchi et al., 2013).

A few days later, on 26 January at 07:31 LT, a small eruptive event preceded the largest explosive eruption recorded in Japan in the last decade (Itano et al., 2011). From 14.50 LT the eruptive activity evolved to a sub-plinian phase, emitting a significant amount of tephra that dispersed towards the SE (Earthquake Research Institute, ERI, Univ.Tokyo, 2013; Earthquake Research Institute, University of Tokyo, 2013; Miyabuchi et al., 2013). This eruptive event, that ended at around 18:30 LT, occurred concurrently with an increase in the amplitude of infrasonic waves and in volcanic tremors (Earthquake Research Institute, ERI, Univ.Tokyo, 2013; Earthquake Research Institute, University of Tokyo, 2013). After this eruption, other two sub-plinian events were recorded by remote video cameras on 27 January between 02:20 and 04:50 LT and 15:30–17:30 LT, respectively (Earthquake Research Institute, ERI, Univ.Tokyo, 2013; Earthquake Research Institute, University of Tokyo, 2013).

According to independent weather radar measurements, performed by the Japan Meteorological Agency, high eruptive columns were produced during the above mentioned eruptions. In particular, the ash plume fluctuated between 6.5–8.5 km asl in the evening of 26 January (during 16:10–18:40 LT), as well as in the early morning (i.e. between 02:00 and 05:00 LT) and in the late afternoon (i.e. between 16:20 and 18:00 LT) of 27 January (Shimbori and Fukui, 2012; Kozono et al.,

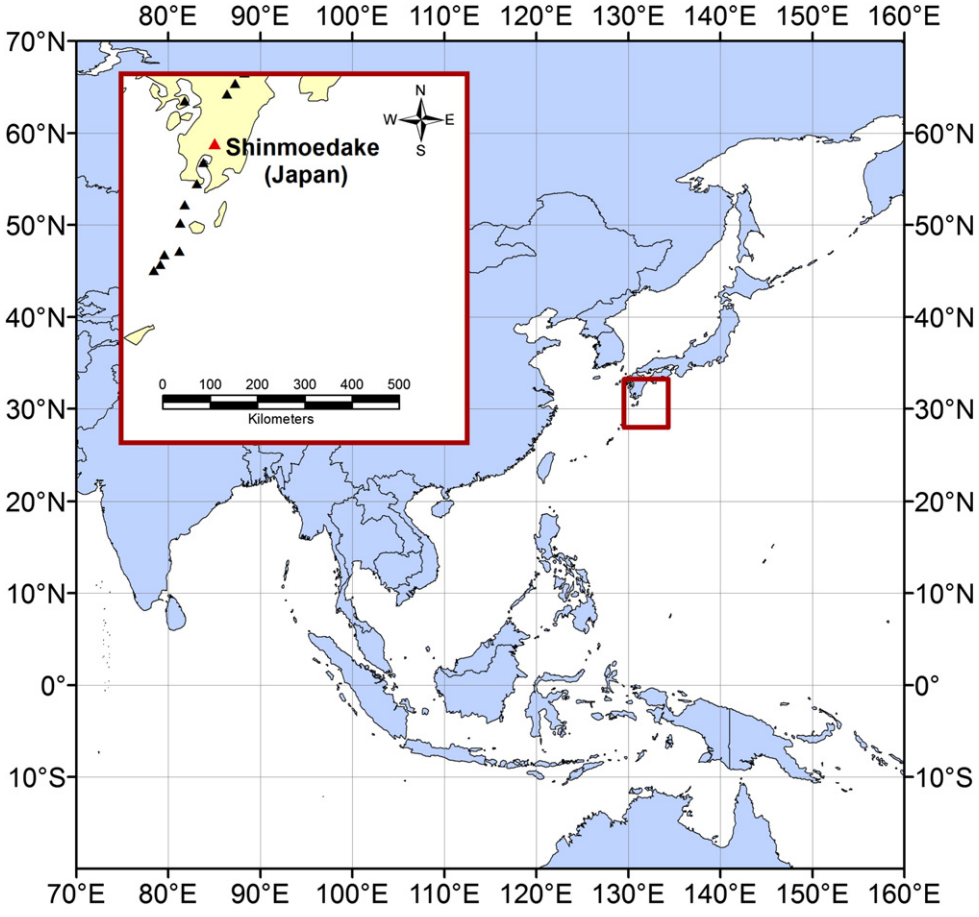

Fig. 1. Shinmoedake volcano geographic localization. In the inset, the area covered by the 171 × 130 MTSAT sub-scenes (i.e. the ROI) is reported.

2013). After these events, another volcanic explosion took place on 28 January (at 12:47 LT), when a flight inspection performed by the Japan Meteorological Agency revealed the presence of lava inside the summit crater, which extended up to 500 m in diameter2 days later (Japan Meteorological Agency, 2013). Fig. 2 reports some images of the 26–27 January eruptions taken by a web camera located at Ohnaminoike, established and maintained by the regional development bureau of Aira and Isa (Kagoshima prefecture, Japan).

Fig. 2. Web camera images of Mt. Shinmoedake eruptions. Date and times (in Local Times) of records are shown on top of each picture. Credits: Regional Development Bureau of Aira and Isa (Kagoshima prefecture).

3. Implemented methodologies

3.1. RST_{VOLC} algorithm: monitoring thermal activity

The RST_{VOLC} algorithm is a specific configuration of the RST approach and is used to study and monitor thermal volcanic activity (Marchese et al., 2011a). The RST approach considers each anomaly in the space–time domain as a deviation from the normal state (i.e. the background), that can be reconstructed by processing homogeneous (i.e. same month, same overpass times) time series of multi-year cloud-free satellite records (Tramutoli, 1998, 2007). The Absolutely Local Index of Change of the Environment (ALICE) is then computed to automatically detect possible anomalous variations of the signal associated to perturbing events. This index, in its general formulation, is defined as:

$$\otimes_V(x,y,t) \equiv \frac{[V(x,y,t)-\mu_V(x,y)]}{\sigma_V(x,y)} \quad (1)$$

where $V(x,y,t)$ is the satellite signal measured at time t and place (x,y), while $\mu_v(x,y)$ and $\sigma_V(x,y)$ respectively represents the temporal mean and standard deviation of the same signal measured in unperturbed conditions.

In the RST_{VOLC} configuration two local variation indexes are used jointly to detect volcanic hot spots. The $\otimes_{MIR}(x,y,t)$ index ($V = T_{MIR}$), introduced in Pergola et al. (2004a), analyzes the brightness temperatures measured in the Medium Infrared band (MIR), at around 3–4 μm, where hot magmatic surfaces (e.g. lava flows), according to Wien's law, reach the peak of their thermal emission. The $\otimes_{MIR-TIR}(x,y,t)$ index ($V = T_{MIR} - T_{TIR}$) is based, instead, on the brightness temperature difference between 4 μm and 11 μm. This index is used in combination with the previous one for increasing filtering capabilities of residual spurious effects (e.g. anomalous fluctuations of the surface temperature associated with weather/climatic factors). The RST_{VOLC} algorithm was first tested on a long time series of infrared AVHRR (Advanced Very High Resolution Radiometer) records, to study Mt. Etna's thermal activity (Marchese et al., 2011a). Later, it was implemented on MODIS (Moderate Resolution Imaging Spectroradiometer) data and then compared to MODVOLC (Wright et al., 2002), showing a similar confidence level of detection, together with a better capability in identifying subtle hot spots (see Lacava et al., 2011). These performances have been further confirmed by a recent retrospective study, where two different phases of thermal unrest, that preceded 1 and 14 September 2004 Mt. Asama (Japan) eruptions, were inferred and characterized by using RST_{VOLC} and MODIS data (Marchese et al., 2012). In this study, the RST_{VOLC} algorithm has been implemented, for the first time, on data provided by geostationary satellites. Performances of this algorithm in monitoring thermal activity of Mt. Shinmoedake during the 26–27 January 2011 eruption are assessed, with results presented in Section 5.1.

3.2. RST_{ASH} algorithm: detecting and tracking volcanic ash clouds

The RST_{ASH} algorithm represents the RST configuration developed to identify and track ash clouds from space. This configuration has been widely described and assessed in previous research papers (e.g. Pergola et al., 2004b; Filizzola et al., 2007). It combines negative values of the $\otimes_{\Delta TIR}(x,y,t)$ index to positive values of the $\otimes_{MIR-TIR}(x,y,t)$ index to detect volcanic ash and to discriminate it from meteorological clouds. The first index, which is based on the brightness temperature difference $\Delta TIR = T_{11\mu m} - T_{12\mu m}$, exploits the inverse spectral behavior of silicate particles at 11 μm and 12 μm wavelengths compared to water droplets and ice (Prata, 1989). The second index (already discussed in the previous section) takes into account instead the different spectral behaviors of ash clouds in the MIR and TIR spectral regions (Pergola et al., 2004b). Different cutting levels of $\otimes_{\Delta TIR}(x,y,t)$ and $\otimes_{MIR-TIR}(x,y,t)$ can be used to identify and track volcanic ash plumes, giving also an indication about regions characterized by a different probability of ash presence (Pergola et al., 2004b). The RST_{ASH} algorithm not using empirical thresholds, whose efficiency is generally affected by several factors, as viewing angles and particle size (Francis et al., 2012), and not requiring any ancillary information is particularly suitable to be used operationally. In spite of some limitations, already discussed in previous works (e.g. Marchese et al., 2011b), this algorithm, offering a good trade-off between reliability and sensitivity (see Pergola et al., 2004b; Filizzola et al., 2007; Piscini et al., 2011), represents then a valid alternative to other satellite-based detection methods (e.g. Prata, 1989; Prata and Grant, 2001; Yu et al., 2001; Ellrod et al., 2003; Pavolonis et al., 2006; Corradini et al., 2008; Lin et al., 2011; Picchiani et al., 2011; Christopher et al., 2012; Francis et al., 2012).

3.3. Cloud-top temperature method: inferring plume height

The plume height is a critical factor for monitoring and forecasting ash dispersion in the atmosphere (e.g. Tupper et al., 2009). Although several methods have been proposed to determine this parameter from satellite data (e.g. Kienle and Shaw, 1979; Glaze et al., 1989; Holasek et al., 1996; Richards et al., 2006; Chang et al., 2010; Zakšek et al., 2013), the accuracy and consistency of its estimations still represent an issue (Webley and Mastin, 2009).

In this work, the cloud-top temperature method has been used to determine the cloud-top height and its temporal fluctuations. This technique assumes that ash clouds have an emissivity close to unity and their top has cooled to the surrounding atmospheric temperature resulting in equilibrium with the ambient air. Therefore, by comparing the minimum plume temperature measured by satellite (generally at 11 μm wavelength) to the atmospheric temperature profiles of the investigated geographic region, the cloud-top height may be determined (Kienle and Shaw, 1979; Sawada, 1987; Glaze et al., 1989; Holasek et al., 1996; Sawada, 2002; Tupper et al., 2004).

The cloud-top temperature method generally provides reasonable estimations of the plume height especially in the presence of opaque clouds. In the presence of optically thinner clouds, more transparent to the thermal radiation coming from the underlying surface, this method becomes instead less reliable. Moreover, for ash clouds near the tropopause a further reduction of its performance is observed (Oppenheimer, 1998; Prata and Grant, 2001).

Taking in mind these limitations, the cloud-top temperature method was implemented in this work after automatically detecting ash pixels. In particular, the minimum plume temperature, measured in the IR1 channel (10.3–11.3 μm) of the MTSAT-2 satellite, was compared to the retrieved atmospheric temperature profiles provided by NCEP/NCAR Reanalysis 1 dataset. The NCEP/NCAR Reanalysis 1 project uses a state-of-the-art analysis/forecast system to perform data assimilation, by using past data from 1948 to the present. The retrieved temperature profiles, as well as other atmospheric parameters (e.g. geopotential height, relative humidity, specific humidity, U wind, V wind), are provided 4-times per day (at 00:00 GMT, 06:00 GMT, 12:00 GMT, and 18:00 GMT) at 17 different pressures levels, with a spatial sampling of 2.5 × 2.5 degrees (Kalnay et al., 1996). The 4-times per day temperature products were analyzed (selecting profiles closest in time to the relative satellite observations) finding the pressure levels at which the coldest plume temperature matched the analyzed atmospheric temperature profile. The curve of the geopotential height was then used to convert the pressure levels in the relative altitudes.

4. Data used

The MTSAT geostationary satellites are owned and operated by the Japanese Ministry of Land, Infrastructure and Transport and by the Japan Meteorological Agency (JMA). The MTSAT-1R satellite, covering East Asia and the Western Pacific region from 140°E above the equator, was operational until 1 July 2010. This satellite currently serves as back-up of MTSAT-2 and performs the services of imagery dissemination and

data collection since the switchover of its imaging function (Tsunomura, 2011). The MTSAT-2 satellite is currently operational in imaging the West Pacific region and it is positioned at 145°E longitude. As the MTSAT-1R, it acquires data in five different spectral bands, from the visible to the thermal infrared, with a spatial resolution of 1 km in the visible band, and 4 km in the infrared bands at nadir view, and with a temporal resolution of 1 h for the full earth's disk observation (Itano et al., 2011). The dissemination of MTSAT data is performed by means of High Rate Information Transmission (HRIT), for full resolution data dissemination, and Low Rate Information Transmission (LRIT) for low resolution data dissemination (Tsunomura, 2011).

The study presented in this paper was carried out extracting a region of interest (ROI) of 171 × 130 pixels in size, centered over Southern Japan (see Fig. 1), from the 1800 × 1800 MTSAT-1R and MTSAT-2 sub-scenes, having a spatial resolution of 0.05°. These data are made freely available online by the Kochi University of Japan (Kochi University, 2013). This work was performed using the MTSAT-1R data of January 2006–2010 (5 years of data) to calculate the spectral reference fields of temporal mean and standard deviation, while the MTSAT-2 data of 26–28 January 2011 were analyzed to detect volcanic features of interest. Although obviously not identical, data coming from the two satellites were actually merged here, with an effect on the presented results that, because of the high similarity of the two data-sets, is considered negligible. The reason for the similarity of the two data-sets is, at least, twofold: i) both data are resampled on the same geographic grid, removing any spatial mismatch between images and smoothing any differences due to stereoscopic effects possibly related to the orbit positional displacement (5°); ii) as declared by the Satellite Program Division of the Japan Meteorological Agency (Satellite Program Division, 2009), and further shown by a recent study (Hayashi, 2012), the spectral characteristics (i.e. spectral response functions, center wavelengths, shapes, bandwidths) of the used infrared channels of both MTSAT satellites are almost identical (with a difference slightly more significant for IR4). As a consequence, the MTSAT-1R and MTSAT-2 infrared brightness temperature values result highly correlated (i.e. R^2 ~ 0.99, bias ~ 0.35 K and RMS ~ 1.5 K), as demonstrated by an independent study performed analyzing 3 days of coincident MTSAT-1R and MTSAT-2 images (Doelling et al., 2013). Thus, we can assert that possible, if any, satellite inter-calibration effects on RST analyses are likely to be negligible with respect to the natural (i.e. environmental + observational) signal fluctuations, and also because of the monthly aggregation of our data-sets.

5. Results

5.1. Thermal monitoring

To study the thermal activity of Mt. Shinmoedake, the RST_{VOLC} algorithm was applied to the MTSAT-2 data acquired from 26 January at 09:00 LT to 28 January at 09:00 LT. An observation time period of 48 h (i.e. 26 January at 00:00 GMT–28 January at 00:00 GMT) was then considered. During the investigated time period detected hot spots clustered in three main time intervals, reflecting the occurrence of three sub-plinian events previously described in Section 2. To better analyze changes in the thermal signal associated with the different eruptive phases of Mt. Shinmoedake, the MIR signal excess (i.e. the difference between the MIR brightness temperature and its temporal mean value), was calculated for a pixel located over the crater area. This signal excess has been plotted in Fig. 3, where red stars indicate thermal anomalies detected by RST_{VOLC}. The figure shows that on 26 January, during the first 7 h of satellite monitoring (i.e. from 09:00 LT to 15:00 LT), the MIR brightness temperature measured in the IR4 (3.5–4.0 μm) channel of MTSAT-2 satellite was comparable to its temporal mean value, not causing any increase in the MIR signal excess. However, at 16:00 LT, as a consequence of the first sub-plinian event, a first sudden and abrupt signal rise was recorded. The analyzed parameter significantly increased

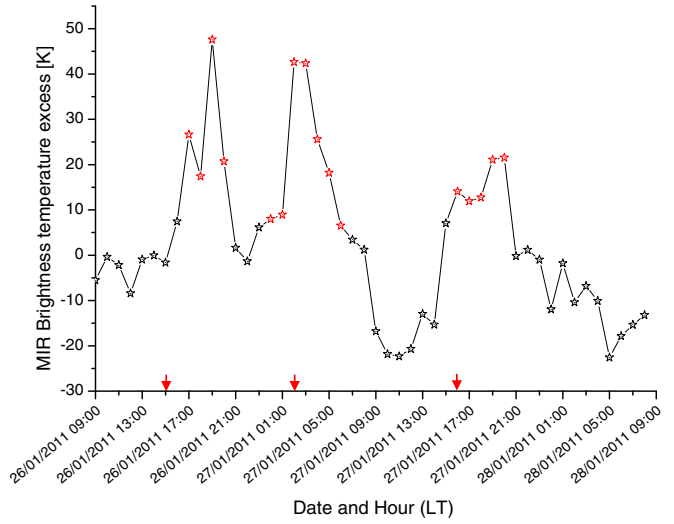

Fig. 3. Temporal trend of the excess of MIR signal, in the period 26 January 2011 at 09:00 LT–28 January 2011 at 08:00 LT, over a crater pixel, with thermal anomalies detected by RST_{VOLC} indicated in red.

until 17:00 LT (when the first hot spot was identified over the crater area) and slightly decreased 1 h later, although the monitored crater pixel continued to be flagged as anomalous by RST_{VOLC}. Even if the first sub-plinian event ended at 18:30 LT (see Section 2), the peak in the MIR excess signal was recorded at 19:00 LT, when two hot spots were detected over the crater area (see Fig. 4*a*). This observation indicates that a different thermal source was probably the cause of hot spots detected by satellite. This thermal source was capable of further increasing the signal measured in the MIR spectral channel of MTSAT-2 satellite. This hypothesis seems to be corroborated by the web camera images reported in Fig. 2, where the occurrence of lava fountains soon after 18:00 LT is shown. Such a volcanic activity, which was still more evident in the following hours, generated the hot spots detected by RST_{VOLC}, although discontinuously (due to an ash plume which probably masked the crater area), until 27 January at 01:00 LT (see also NASA, 2013a). Indeed, 1 h later, another sudden and strong increase in the excess of MIR signal occurred, indicating the onset of the second sub-plinian event, in good agreement with field observations. This eruptive activity reached its peak, in terms of the monitored parameter, at 03:00 LT and 04:00 LT, when the number of detected hot spots slightly increased (from 2 to 3 anomalous pixels identified over the crater area; see Fig. 4*b*). Afterwards, the MIR signal excess progressively decreased, although the crater pixel was still flagged as anomalous by RST_{VOLC} until 1 h later the end of second sub-plinian eruption (i.e. at 06:00 LT). The web camera images reported in Fig. 2 seem to confirm also this satellite observation showing the end of the thermal activity at around 06:30 LT. In the following hours the MIR signal excess continued to decrease assuming negative values starting from 08:00 LT, as a consequence of meteorological clouds masking the crater area. Clouds affected the analyzed satellite observations until 14:00 LT (see Fig. 3). One hour later, between 15:00 and 16:00 LT another evident increase in the MIR signal excess (although less abrupt than before) was recorded, reflecting the beginning of the third sub-plinian event. Although this eruption ended at around 18:00 LT (see Section 2), the crater area remained thermally active until 20:00 LT. This observation indicates that a lava dome, revealed in the morning of 28 January by an independent flight inspection (Miyabuchi et al., 2013), was probably already present inside the crater since the evening of the day before. It can be then speculated that this thermal feature was capable of generating volcanic hot spots, that were once again discontinuously identified by satellite because of meteorological clouds affecting crater area (from 27 January at 21:00 LT). Fig. 3 gives then information about changes in

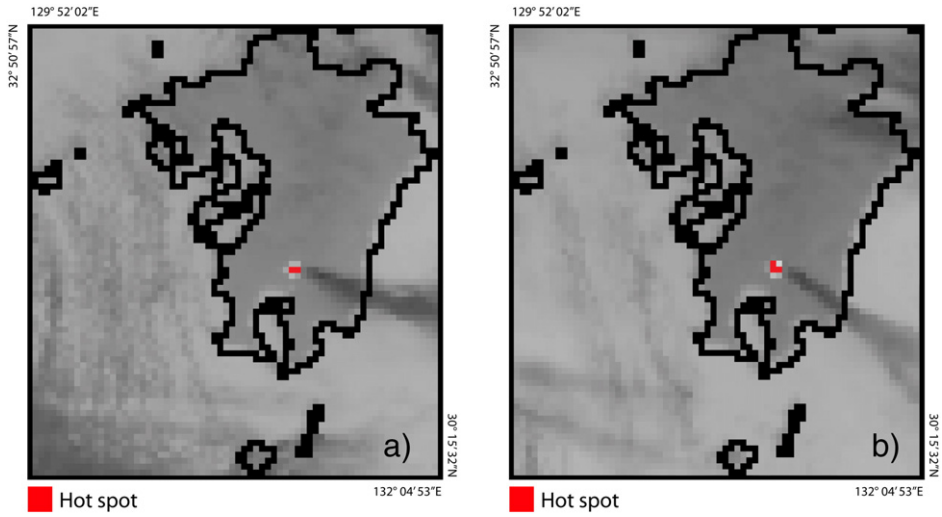

Fig. 4. Hot spots (in red) detected by RST_{VOLC} on Mt. Shinmoedake crater area. *a)* 26 January at 10:00 GMT (19:00 LT); *b*) 27 January at 18:00 GMT (03:00 LT).

thermal activity that occurred at Mt. Shinmoedake during the investigated time period. It shows that the peak in the MIR signal excess was reached during the lava fountain activity, independently observed on the ground since the afternoon of 26 January. Furthermore, the same figure shows that among sub-plinian events of Mt. Shinmoedake, the third one, which occurred in the afternoon of 27 January, produced a lower increase in the MIR signal excess. This is particularly evident also considering that the first and the third sub-plinian events occurred almost at the same hours. On the basis of this analysis it is then possible to speculate that the third sub-plinian phase at Mt. Shinmoedake was probably less powerful than the previous ones.

5.2. Ash cloud detection

In Fig. 5, a time sequence of infrared MTSAT-2 images (from 26 January at 07:00 GMT to 27 January at 07:00 GMT) processed by RST_{ASH} is reported. These RST_{ASH} maps were generated by processing a signal measured in the IR1 (10.3–11.3 μm), IR2 (11.5–12.5 μm) and IR4 (3.4–4.1 μm) channels of MTSAT satellites. The figure shows that the ash cloud emitted by Mt. Shinmoedake was detectable by satellite from 08:00 GMT, i.e. 2 h after the beginning of first sub-plinian eruption. The early detection of the plume was probably affected by its opacity as well as by a possible cold background effect. As can be seen looking at the generated RST_{ASH} maps, the ash plume was initially E directed and already extended over 30°N in latitude and 135°E in longitude at 11:00 GMT. In the following hours it separated in two different branches, as a consequence of the wind direction at different atmospheric altitudes, as indicated by the upper air sounding at Kagoshima (see Itano et al., 2011; Hashimoto et al., 2012). From 19:00 GMT (27 January at 03:00 LT), when the second sub-plinian eruption was in progress at volcano, the ash plume moved also in the NE direction. A few hours later, a thick cloud coverage affected the coast of Southern Japan and consequently only the distal part of the plume was identified by RST_{ASH}. Such an effect was particularly significant on satellite imagery of 27 January at 02:00–03.00 GMT (11:00–12:00 LT). In the following hours the proximal part of the plume was once again detectable, with the volcanic ash that progressively dispersed outside the ROI, moving in the SE direction.

This image sequence reports an entire day of satellite observations (24 h), over 36 h of MTSAT-2 data analyzed, revealing the presence of volcanic ash over the investigated geographic area. The figure shows that, even if the ash plume was not completely detected by RST_{ASH} (also because of meteorological clouds), it was in general well tracked from space. In addition, only few false positives were generated over the analyzed satellite scenes, as confirmed by a comparison with some independent satellite-based aerosol products (e.g. SCIAMACHY AI; MODIS AOD daily product), not shown here (see Goddard Earth Science Data and Information Service Center, 2013; Support to Aviation Control Service, 2013).

To give a better overview of ash dispersion over the ROI, during the first 24 h of satellite monitoring, the mean value of $\otimes_{\Delta TIR}(x,y,t)$ index has been reported in Fig 6. The figure shows that volcanic ash dispersed over a wide portion of the monitored geographic area, resulting in particular more persistent over the coastal area of Southern Japan. In this area, lower critical levels of $<\otimes_{\Delta TIR}(x,y,t)>$ index were indeed recorded. However, these critical values of RST_{ASH} index could reflect also the different distribution and/or concentration of finer ash particles over the ROI. In particular, ash particles having a diameter less than 10 μm, that generally cause negative values of BTD signal (see Wen and Rose, 1994), probably impacted also on the values of $<\otimes_{\Delta TIR}(x,y,t)>$ index. The finer ash particles, characterized by a longer residence time in the atmosphere and dispersing over long distances, provided a negligible contribution to the tephra fall out during Mt. Shinmoedake eruptions, as indicated by the analysis of tephra amount deposits independently reported in previous works (Furukawa et al., 2011; Hashimoto et al., 2012; Maki et al., 2012).

5.3. Cloud-top height estimations

Fig. 7 reports the temporal fluctuations of cloud-top height estimated applying the cloud-top temperature method to the ash pixels previously identified by RST_{ASH}. As can be seen from the figure, during the investigated eruptions the ash plume strongly fluctuated in altitude. It reached its maximum height, estimated at around 7.4 km asl, on 26 January at 18:00 LT and on 27 January at 05:00 LT (i.e. during the first and second sub-plinian phase). The third sub-plinian event produced, instead, a lower eruptive column, which extended up to about 6.4 km asl. Besides these peaks, the plot of Fig. 7 shows a slight and continuous increase of cloud top height recorded before the second sub-plinian event, that lasted a few hours (i.e. between 26 January at 23:00 LT and 27 January at 02:00 LT). Moreover, a sharp and isolated peak can be also observed between the second and the third sub-plinian events (i.e. on 27 January at 13:00 LT). In the first case, the slight increase of the cloud-top height seems to be consistent with the occurrence of smaller eruptions that, according to ground-based observations, produced eruptive columns fluctuating between 3 and 5 km asl (Shimbori and Fukui, 2012). On the contrary, the abrupt increase observed in the second case was probably a consequence of the

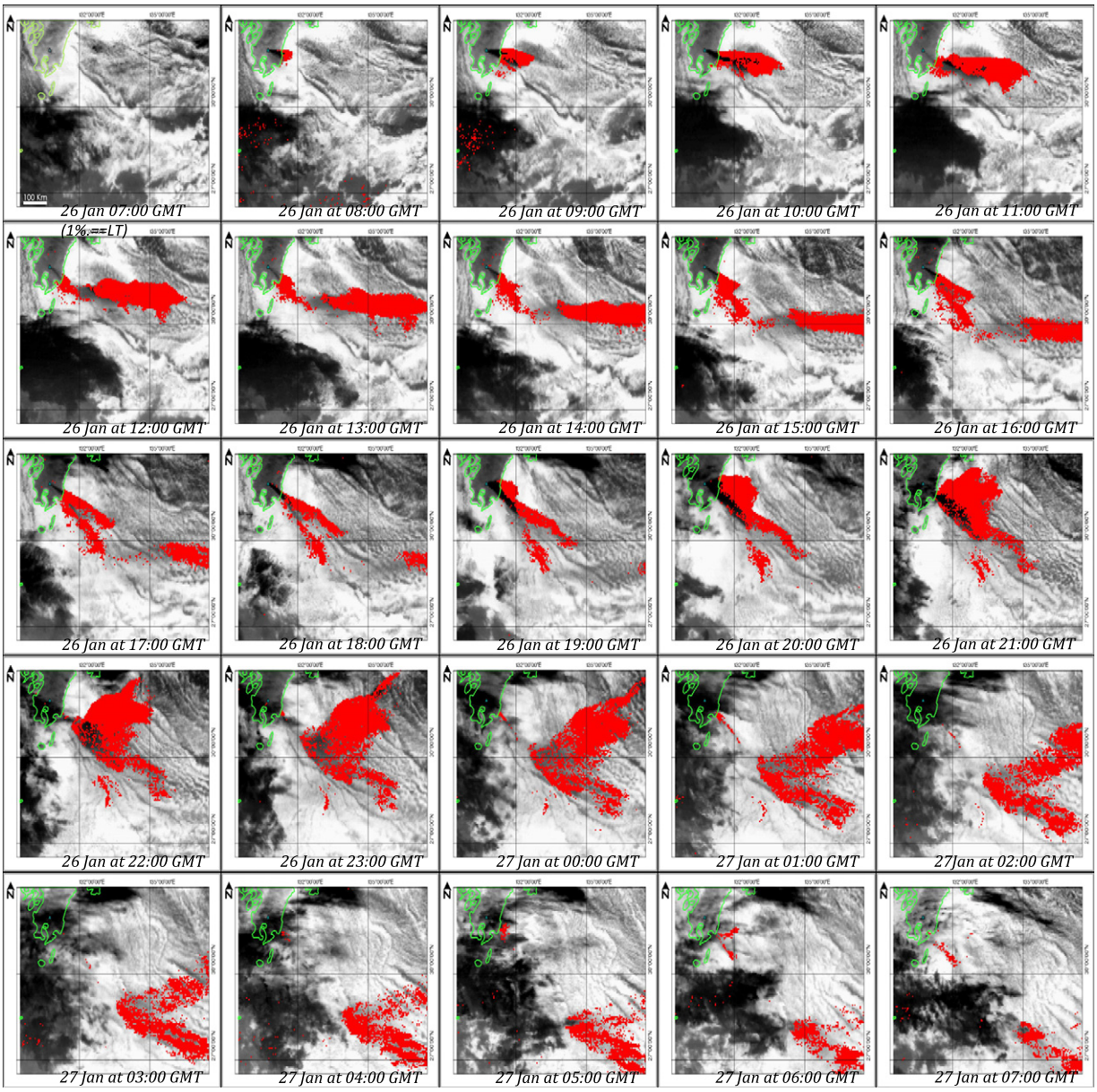

Fig. 5. Ash cloud emitted by the Shinmoedake volcano between 26 January 2011 at 08:00 GMT (17:00 LT) and 27 January 2011 at 07:00 GMT (16:00 LT) and detected by RST_{ASH} on infrared MTSAT data (red pixels).

meteorological clouds affecting ash detection. Indeed, as discussed in the previous section, on 27 January between 09:00 and 12:00 LT, a thick cloud coverage masked the proximal portion of the plume. Because of this cloud masking effect the minimum plume temperature was retrieved in an area more distant from the source, and where the plume was presumably optically thinner. These conditions probably affected, in a more significant way, the accuracy of cloud-top height estimations (as better discussed later). Starting from 13:00 LT the proximal region of the plume was, instead, less affected by meteorological clouds. Consequently, the coldest plume temperature was better retrieved and an apparent increase in the cloud-top height occurred.

The temporal fluctuations of cloud-top height determined in this work indicate that three main ash injection events occurred at Mt. Shinmoedake, whose effects lasted about 12 h each (marked A, B, C in Fig. 7). They reflected the occurrence of a series of eruptive events, independently observed also by ground-based systems (see Section 2).

The values of cloud-top heights reported in this work, although compatible with the information provided by Tokyo VAAC (Tokyo VAAC, 2013), appear in general lower than those provided by independent weather radar measurements, for which the ash plume reached a maximum altitude of about 8.5 km during the sub-plinian phases (see also Hashimoto et al., 2012). In particular, the main differences with aforementioned weather radar observations seem to characterize especially the third sub-plinian event. In this case, a more significant deviation in the cloud-top height compared to previous eruptions (~2 km), has been recognized. To better assess these differences, a manual inspection of infrared satellite records, devoted to evaluate the impact of the used ash detection scheme on retrieved plume altitudes, has been performed first. By this analysis we can assert that the possible plume height underestimation was not a consequence of detection issues. In particular, the plume region closer to the source and extending over land areas, although not identified by RST_{ASH}, had a negligible impact on the values of cloud-top height estimated here. This is clearly indicated by the difference in altitude for the third sub-plinian event resulting less than 300 m. Therefore, it is then reasonable to suppose that the main causes of such a possible underestimation were the optical (e.g. ash plume

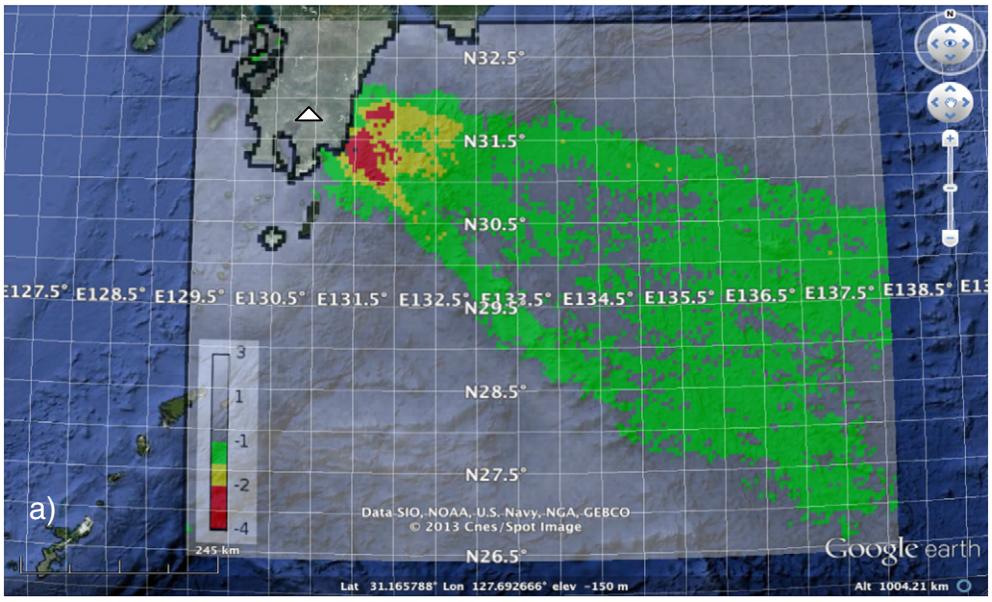

Fig. 6. Mean value of the $\otimes_{\Delta TIR}(x,y,t)$ index calculated over the same time period of Fig. 5, with lower critical levels of this index reflecting region where higher was probably the persistence of ash.

not completely opaque) and/or thermal (e.g. volcanic cloud not in thermodynamic equilibrium with surrounding atmosphere) properties of the plume. However, the hypothesis of a lower ash cloud height during the third sub-plinian eruption cannot be completely excluded, as suggested by an additional analysis also reported in this paper and discussed in Section 6.

5.4. Estimates of discharge rate, erupted volume and mass eruption rate

By the values of the cloud-top height reported in this work, the discharge rate, giving information about eruption intensity (Walker, 1980) can be roughly estimated, by using some empirical formulations reported in literature. These relations (e.g. Settle, 1978; Wilson et al., 1978; Sparks et al., 1997; Mastin et al., 2009), applied by different authors to several past eruptions, provide estimates of discharge rate with errors generally around ±25% (see Mastin et al., 2009).

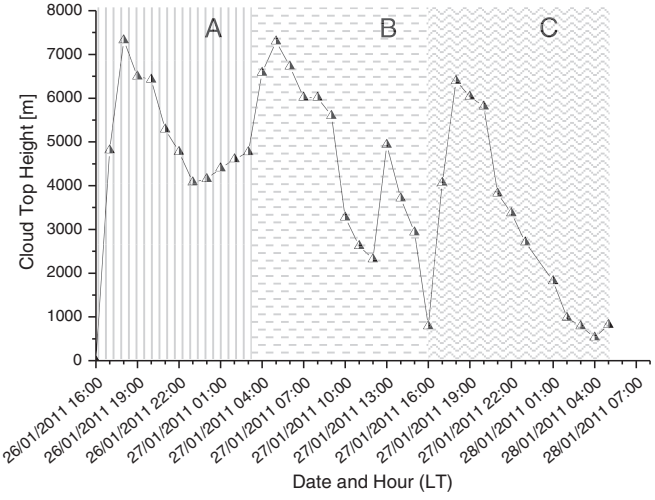

Fig. 7. Temporal fluctuations of the cloud-top height, estimated on the entire period of satellite observations (36 h), i.e. between 26 January at 17:00 LT and 28 January at 05:00 LT, with three main ash periods (A, B, C), having a time duration of about 12 h each, discriminated over the plot (see text).

In this work, to determine the discharge rate V (m^3/s) from the cloud-top height H (km) the known empirical formulation proposed by Sparks et al. (1997) has been used:

$$V = (H/1.67)^{1/0.259}. \quad (1)$$

The discharge rate was estimated here for each sub-plinian event of Mt. Shinmoedake which produced a strong increase in the cloud-top height, as shown in Fig. 7, and whose times of occurrence appear compatible with time of observation of high eruptive columns by means of independent weather radar measurements (see Section 2). Table 1 reports the results of these estimations for the three sub-plinian events indicated here as phase I (26 January at 17:00–18:00 LT), phase II (27 January at 03:00–05:00 LT) and phase III (27 January at 16:00–18:00 LT) to be compared with the results reported in previous independent works.

The values of the discharge rates of 361 m^3/s (phase I), 554 m^3/s (phase II) and 209 m^3/s (phase III) determined in this work are lower than those reported in a previous independent study, with the main differences characterizing the third sub-plinian event (because of the lower plume height estimation, see previous section). However, also considering the associated error, these values are still compatible with the average discharge rate of 610–1060 m^3/s for phases I–II and of 330–670 m^3/s for phase III, independently derived from weather radar observations (see Kozono et al., 2013). Moreover, they are also

Table 1
Discharge rate (m^3/s) estimated, implementing the empirical formulation proposed by Sparks et al. (1997), for the three sub-plinian events of Mt. Shinmoedake respectively indicated as phase I (26 January 17:00–18:00 LT), phase II (27 January 02:00–05:00 LT) and phase III (27 January 16:00–18:00 LT). Erupted volume (m^3) derived from discharge rate values considering the different time duration of each sub-plinian phase of the volcano (see text). Mass eruption rate (kg/s) estimated considering an ash density ρ_a of 2600 kg/m^3.

	Phase I	Phase II	Phase III
Discharge rate [m^3/s]	361	554	209
Total erupted volume [m^3]	2.6×10^6	6.0×10^6	2.3×10^6
Erupted mass rate [kg/s] (assuming p = 2600 kg/m^3)	9.4×10^5	1.4×10^6	5.4×10^5

consistent with the values of 450–563 m^3/s (phase I), 592–741 m^3/s (phase II) and 481–602 m^3/s (phase III) that were independently derived by means of geodetic and SAR (Synthetic Aperture Radar) data (Kozono et al., 2013).

It should be stressed that also the values of total erupted volume determined in this work for each explosive phase (see Table 1), considering the relative time duration (derived on the basis of infrared satellite observations), are comparable with independent estimates of the same parameter (see Maeno et al., 2012; Kozono et al., 2013). More in detail, for the second sub-plinian event, as well as for the smaller eruptions which occurred since the evening of 26 January (for which an erupted volume of 1.8×10^6 m^3 has been determined), the estimates of the erupted volume reported here fit fairly well with those of previous studies (see Kozono et al., 2013).

Finally, assuming that the emitted ash plume was composed mainly of ash particles having a density of 2.6 g/cm^3 (Neal et al., 1994), the mass eruption rate (kg/s) was also determined. The values of this parameter, reported in Table 1, are compatible with those of $7 \pm 3 \times 10^5$ kg/s independently estimated by other authors (see Maeno et al., 2012).

6. Discussion and conclusions

In this paper, a retrospective analysis of the Mt. Shinmoedake eruptions of 26–27 January 2011 has been presented. Data provided by Japanese geostationary satellites were used to monitor thermal volcanic activity, to identify and track volcanic ash and to estimate the cloud-top height, inferring eruption features. The sub-plinian events of Mt. Shinmoedake produced a sudden and abrupt increase in the MIR signal, generating hot spots over the crater area that were timely identified by RST_{VOLC}. Moreover, the lava fountain activity also recorded by remote video cameras, as well as the lava dome independently observed by a flight inspection performed on 28 January 2011, generated thermal anomalies correctly detected by the algorithm used in this work. These results confirm the high performance of RST_{VOLC} and demonstrate its successful exportability on data provided by geostationary satellites.

Regarding the ash plume emitted during the above mentioned eruptions, it was identified by the RST_{ASH} algorithm 2 h after the beginning of the first sub-plinian eruption, when it was probably larger in size

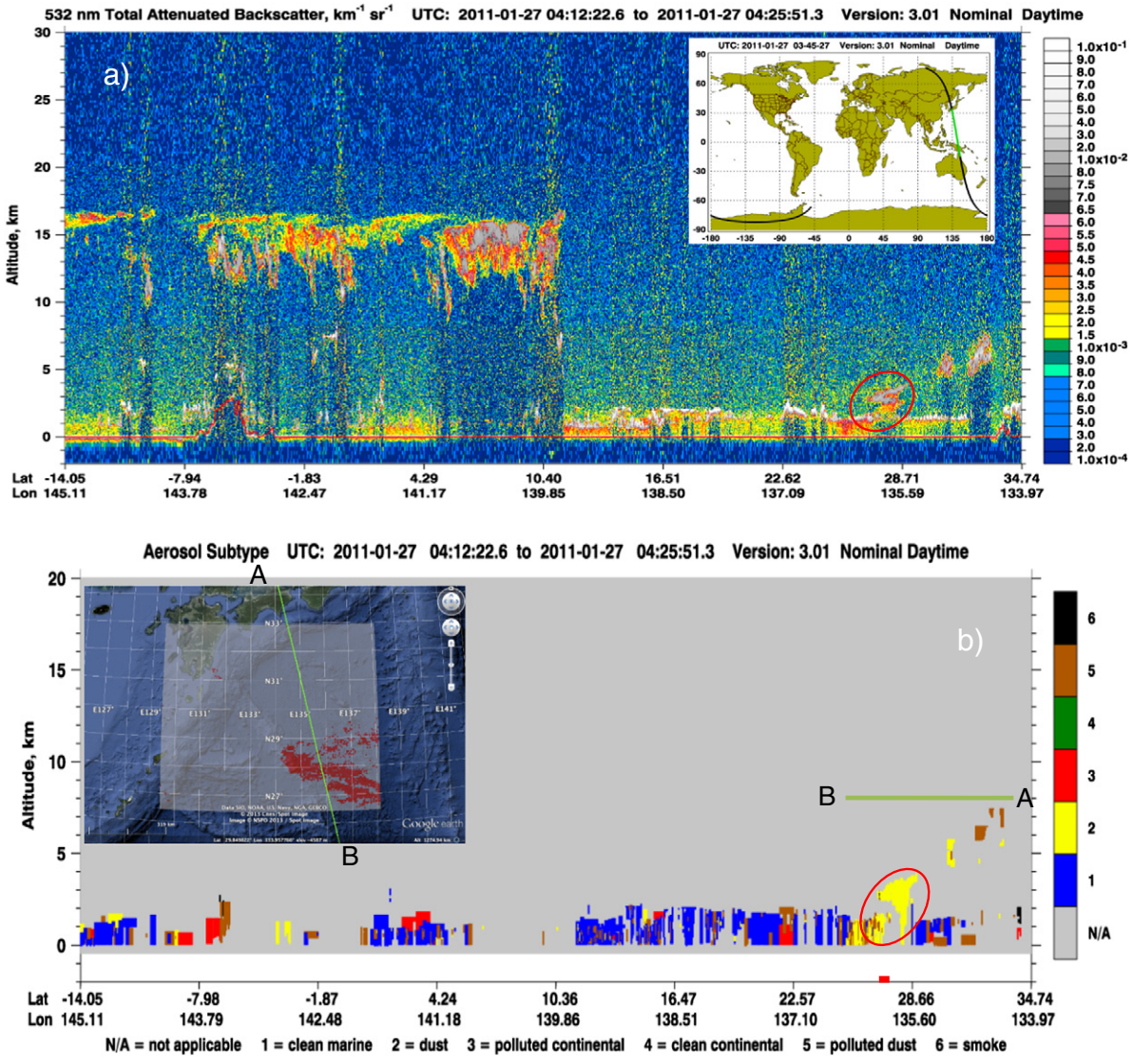

Fig. 8. a) Color-modulated, altitude-time image of CALIPSO 532 nm Total (Parallel + Perpendicular) attenuated backscatter (km^{-1} sr^{-1}) profile of 27 January 2011 (between 04:12 and 04:25 GMT) along the portion (in green) of the orbit track reported in the inset; b) Aerosol sub-type profile with indication of the "dust" layer (in the red ellipse) along the A–B transect (see inset) corresponding to the volcanic ash detected by RST_{ASH} on MTSAT-2 data of 27 January at 04:00 GMT.

and dispersed also over sea areas. The possible low temperature contrast between the cloud-top and the underlying land surface, the optical properties of the plume and the diffuse cloud coverage which affected the West Pacific region, represented the main factors impacting on the identification of ash clouds from space. Because of these issues, the ash plume was not completely described in terms of shape, size and extent, although its space–time evolution was in general well tracked exploiting the high temporal resolution of MTSAT-2 satellite.

The values of cloud-top height reported in this work, derived by applying a method largely used in literature, although lower than those independently provided by weather radar measurements, appear reasonable, also on the basis of information that were provided by the Tokyo VAAC. The possible underestimation of cloud-top height compared to weather radar measurements was presumably a consequence of the intrinsic limitations of cloud-top temperature method. Such an underestimation was more significant for the third sub-plinian event (with a relative error of about 25%) that, on the basis of results reported here, was the least intense. Since detection issues had a negligible impact on accuracy of cloud-top estimations performed here (as revealed by a manual inspection of infrared satellite records), it can be speculated that the lower peak in the cloud-top height recorded during this event was the consequence of an ash cloud optically thinner than before.

To better assess the impact of plume transparency on the performance of the cloud-top temperature method, a comparison of RST_{ASH} map of 27 January at 04:00 GMT with the CALIOP data available at about same hour for the investigated geographic area (National Aeronautics and Space Administration, 2013b) is reported in Fig. 8. CALIOP is a spaceborne two-wavelength polarization lidar representing the primary instrument on the Cloud-Aerosol Lidar and Infrared Pathfinder Satellite Observations (CALIPSO) of the NASA "A-train" constellation satellite (Winker et al., 2004, 2007, 2009). This instrument, based on a Nd:YAG laser operating at 1064 nm and 532 nm, provides high resolution vertical profiles of clouds and aerosols along with their microphysical and optical properties (Winker et al., 2004, 2007). CALIOP data were already used to study recent volcanic eruptions (e.g. Carn et al., 2009; Stohl et al., 2011), since they perform direct measurements of the plume height, with improvements compared to indirect estimations of the same parameter (Carn et al., 2009). Fig. 8*a* reports the total (parallel + perpendicular) attenuated backscattered ($km^{-1}\ sr^{-1}$) profile along the orbit track of CALIPSO of 27 January between 04:12–04:25 GMT showing the presence of an aerosol layer between 2 and 4 km in altitude, in correspondence of detected volcanic ash. This layer was classified as "dust" on the aerosol sub-type profile (A–B) reported in Fig. 8*b*. This comparison well corroborates RST_{ASH} detection over the same geographic area, but also shows that if the cloud-top temperature method was applied to this region of the plume (distant more than 600 km from the source, and where volcanic ash was presumably more dispersed in the atmosphere) the relative error in estimating its height was around 60%. This analysis confirms that the cloud top temperature method tends to provide less accurate estimates of the plume height in the presence of ash clouds optically more transparent (see also Webley and Mastin, 2009). It should be stressed that, although a higher transparency of the plume could have determined the lower peak in the cloud-top height estimated here for the third sub-plinian event, such an hypothesis requires other observations to be verified. Moreover, it is interesting to note as the plot of Fig. 9, reporting the ash affected areas calculated multiplying the number of detected ash pixels by the image pixel size, indicates that the third sub-plinian event was probably characterized by a lower dispersive power than previous ones. The dispersive power, representing the area of tephra dispersal, is one of parameters together with eruption intensity used to characterize explosive eruptions and representing a direct function of column height and fragmentation of ejecta (see Walker, 1980; Suzuki, 1983). Fig. 9 shows that during the period C, determined by the third sub-plinian event, volcanic ash was dispersed over a less extended area, resulting lower than 45% of period A

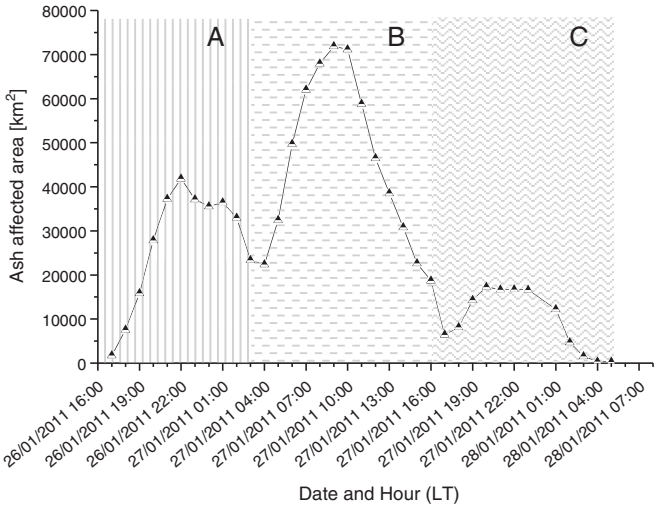

Fig. 9. Temporal trend of the area (km^2) covered by ash during 26 January at 16:00 LT (07:00 GMT) – 28 January at 05:00 LT (27 January at 20:00 GMT), with the indication of the three ash injection periods (A, B, C) previously discriminated in Fig. 7.

(for which, as opposed to period B, no cumulated effects occurred). Considering that the dispersive power is closely related to the eruption intensity (Carey and Sigurdsson, 1989), this plot seems to corroborate the lower cloud-top height, and consequently the lower discharge rate, estimated here for the third sub-plinian event. In addition, results of thermal monitoring reported in Section 5.1 (see Fig. 3) seem to further confirm such a speculation, showing that the third sub-plinian eruption, although still capable of generating hot spots over the crater area, produced a less evident increase in the excess of MIR signal compared to previous sub-plinian phases.

The reasonable estimations of plume height reported in this work are indirectly confirmed also by a series of simulations performed using the HYSPLIT (Hybrid Single Particle Lagrangian Integrated Trajectory Model) Volcanic Ash Model (Draxler and Rolph, 2013; Rolph, 2013). An example of these simulations is reported in Fig. 10. The figure shows that, using the plume height estimated here at the beginning of first sub-plinian eruption (i.e. on 26 January at 08:00 GMT) as input to HYSPLIT, the forecasted and observed (from satellite) ash cloud trajectories were compatible both in terms of plume direction and extent. This is evident looking at the RST_{ASH} map generated 6 h after the time of the beginning of the simulation (i.e. on 26 January at 14:00 GMT; see Fig. 10).

In spite of some limitations affecting algorithms and methods used in this work (as a difficulty in completely detecting the plume and possible inaccuracies in the estimate the cloud-top height from infrared satellite data), this study shows that infrared MTSAT-2 data, if adequately processed, may give an important contribution for the surveillance of active volcanoes located in the West Pacific region.

More in general, this work confirms capabilities of high temporal resolution satellites in providing timely alerts about eruption onsets, in recognizing different thermal phases of volcanoes, and in well characterizing eruption features (see also Webley et al., 2012). It also shows that information about the cloud-top height may be potentially provided in real time when geostationary satellite data are used (with an accuracy depending on the implemented methods). They may significantly support activities devoted to monitoring and forecasting ash dispersion in the atmosphere, contributing to better mitigating of the impact of explosive eruptions on air traffic, in the framework of operational warning systems.

Acknowledgments

This study has been performed using MTSAT-1R data provided by Kochi University of Japan, available at http://weather.is.kochi-u.ac.jp/

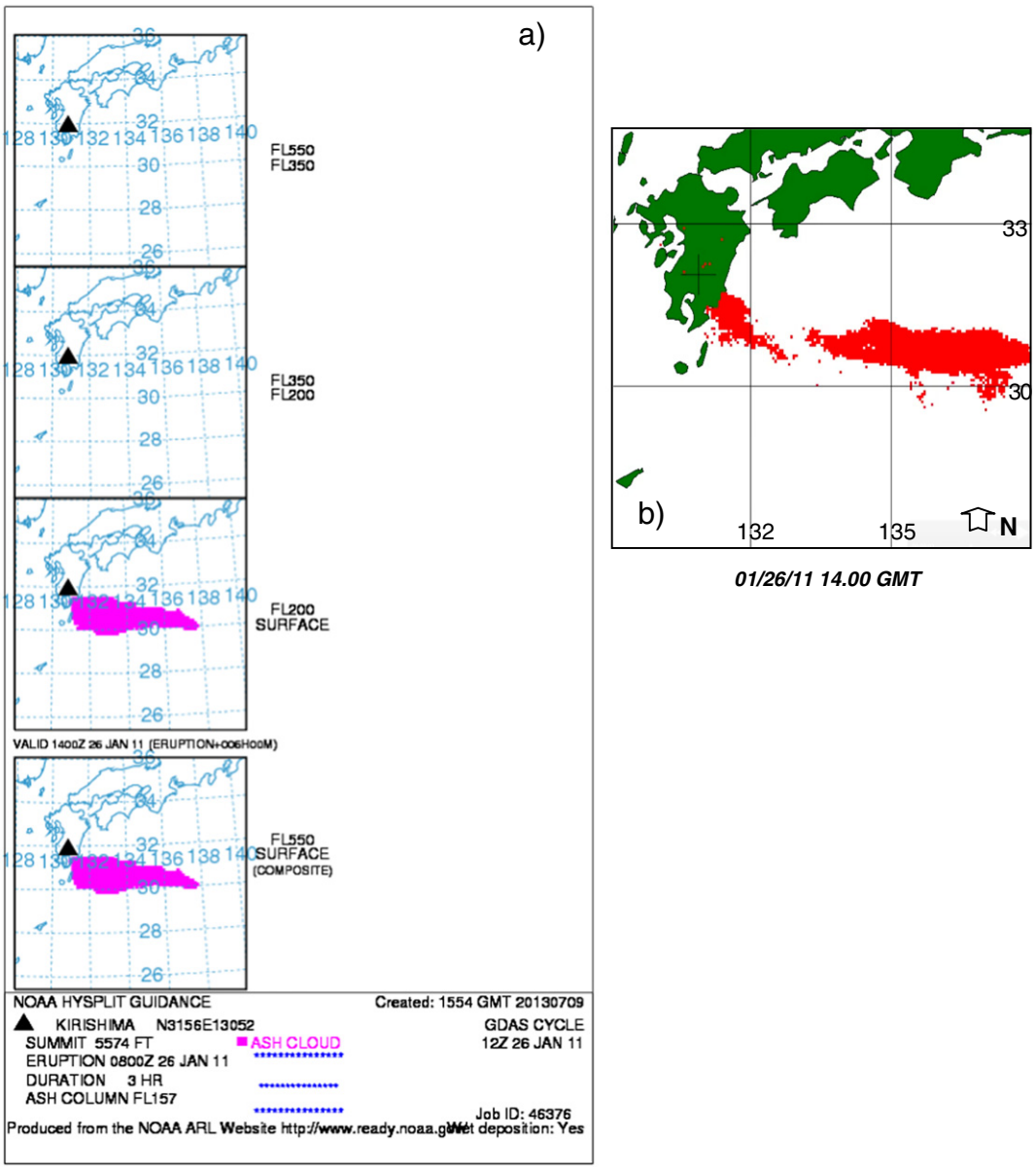

Fig. 10. a) Forecast of ash plume path (at 6 h) derived using the cloud-top height estimated on 26 January at 08:00 GMT (z ~ 4800 m) as input to the HYSPLIT Volcanic Ash model; b) RST_{ASH} map of 26 January 2011 at 14:00 GMT.

archive-e.html. The NCEP Reanalysis data were provided by the NOAA/OAR/ESRL PSD, Boulder, Colorado, USA, from their Web site at http://www.esrl.noaa.gov/psd/. The authors gratefully acknowledge the NOAA Air Resources Laboratory (ARL) for the provision of the HYSPLIT transport and dispersion model and/or READY website (http://www.arl.noaa.gov/ready.php) used in this publication.

The authors want to acknowledge the regional development bureau of Aira and Isa (Kagoshima prefecture) for permission to use their photographs and their efforts to maintain the Web camera.

References

Carey, S., Sigurdsson, H., 1989. The intensity of plinian eruptions. Bull. Volcanol. 51, 28–40.

Carn, S.A., Pallister, J.S., Lara, L., Ewert, J.W., Watt, S., Prata, A.J., Thomas, R.J., Villarosa, G., 2009. The unexpected awakening of Chait'en Volcano, Chile. EOS Trans. Am. Geophys. Union 90, 25. http://dx.doi.org/10.1029/2009EO240001.

Chang, F.L., Minnis, P., Lin, B., Khaiyer, M.M., Palikonda, R., Spangenberg, D.A., 2010. A Modified Method for Inferring Upper Troposphere Cloud Top Height Using the GOES 12 Imager 10.7 and 13.3.

Christopher, S.A., Feng, N., Naeger, A.R., Johnson, B.T., Marenco, F., 2012. Satellite remote sensing analysis of the 2010 Eyjafjallajokull volcanic ash cloud over the North Sea during May 4–May 18, 2010. J. Geophys. Res. http://dx.doi.org/10.1029/2011JD016850.

Corradini, S., Spinetti, C., Carboni, E., Tirelli, C., Buongiorno, M.F., Pugnaghi, S., Gangale, G., 2008. Mt. Etna tropospheric ash retrieval and sensitivity analysis using Moderate Resolution Imaging Spectroradiometer measurements. J. Appl. Remote Sens. 2, 023550. http://dx.doi.org/10.1117/1.3046674.

Doelling, D., Khlopenkov, K., Okuyama, A., 2013. Development of the MTSAT-1R visible footprint point spread function. 19th CERES Science Team Meeting NASA-Langley, Hampton, VA, May 7–9, 2013 (Available at http://ceres.larc.nasa.gov/documents/STM/2013-05/29-CERES_doelling_MTSAT1_2013_05b.pdf).

Draxler, R.R., Rolph, G.D., 2013. HYSPLIT (HYbrid Single-Particle Lagrangian Integrated Trajectory) model access via NOAA ARL READY. Website (http://ready.arl.noaa.gov/HYSPLIT.php) NOAA Air Resources Laboratory, Silver Spring, MD.

Earthquake Research Institute (ERI), Univ.Tokyo, 2013. Eruption of Shinmoe-dake (Kirishima volcano group), Japan, 2011. http://outreach.eri.u-tokyo.ac.jp/eqvolc/201101_shinmoe/eng/.

Earthquake Research Institute, University of Tokyo, 2013. Eruption of Shinmoe-dake (Kirishima volcano group), Japan, 2011. Available at http://outreach.eri.u-tokyo.ac.jp/eqvolc/201101_shinmoe/eng/.

Ellrod, G.P., Connell, B.H., Hillger, D.W., 2003. Improved detection of airborne volcanic ash using multispectral infrared satellite data. J. Geophys. Res. 108, 4356.

ESA-EUMTSAT, 2010. Workshop on the 14 April to 23 May 2010 eruption at the Eyjafjöll volcano, South Iceland. In: Zehner, C. (Ed.), Monitoring Volcanic Ash from Space. ESA/ESRIN.

Filizzola, C., Lacava, T., Marchese, F., Pergola, N., Scaffidi, I., Tramutoli, V., 2007. Assessing RAT (Robust AVHRR Technique) performances for volcanic ash cloud detection and monitoring in near real-time: the 2002 eruption of Mt. Etna (Italy). Remote Sens. Environ. 107 (3), 440–454.
Francis, P.N., Cooke, M.C., Saunders, R.W., 2012. Retrieval of physical properties of volcanic ash using Meteosat: a case study from the 2010 Eyjafjallajökull eruption. J. Geophys. Res. - Atmos. (1984–2012) 117 (D2).
Furukawa, R., Geshi, N., Nakano, S., Hoshizumi, H., Takarada, S., Takeuchi, S., Toshida, K., Tajima, Y., Tsutsui, M., 2011. Urgent survey of eruptive deposit in January, 2011, from Shinmoedake volcano, Mt. Kirishima, South Kyushu, Japan. Proceedings of the JGU meeting 2011, SVC050-05 (in Japanese).
Geshi, N., Saito, G., Tomiya, A., Miyagi, I., Furukawa, R., Nakano, S., Hoshizumi, H., Takarada, S., 2011. Magma of the January 2011 eruption of Shinmoedake, Kirishima Volcano. Japan Geoscience Union Meeting 2011 Abstracts, SVC050-04.
Glaze, L.S., Francis, P.W., Self, S., Rothery, D.A., 1989. The 16th September 1986 eruption of Lascar volcano, north Chile: satellite investigations. Bull. Volcanol. 51, 149–160.
Goddard Earth Science Data and Information Service Center, 2013. Available at http://disc.sci.gsfc.nasa.gov/.
Hashimoto, A., Shimbori, I., Fukui, K., 2012. Tephra fall simulation for the eruptions at Mt. Shinmoe-dake during 26−27 January 2011 with JMANHM. SOLA 8, 037–040. http://dx.doi.org/10.2151/sola.2012-010.
Hayashi, M., 2012. Recent status and development of atmospheric motion vectors at JMA. 11th International Winds Workshop, Auckland, New Zealand, 20–24 February, 2012.
Holasek, R.E., Self, S., Woods, A.W., 1996. Satellite observations and interpretation of the 1991 Mount Pinatubo eruption plumes. J. Geophys. Res. 100, 8469–8487.
Imura, R. and Kobayashi, T., 2001. Geological map of Kirishima Volcano (1:50,000). Geological Map of Volcanoes 11, Geological Survey of Japan (in Japanese with English abstract).
International Civil Aviation Organization (ICAO), 2007. International Airways Volcano Watch Operations Group. (IAVWOPSG) Third Meeting Bangkok, Thailand, 19 to 23 March 2007.
Itano, T., Matsuura, Y., Eguchi, T., 2011. Tracking of volcanic ash emanated through Shinmoedake eruption by using MTSAT split-window imagery. The Second Asia/Oceania Meteorological Satellite User's Conference 6–9 December 2011 Mita Kaigisho, Tokyo, Japan, 2011.
Japan Meteorological Agency, 2005. National Catalogue of the Active Volcanoes in Japan, Third edition. (635 pp. in Japanese).
Japan Meteorological Agency, 2013. Monthly activity report January (2013). Available at http://www.seisvol.kishou.go.jp/tokyo/eng/volcano_activity/2011/2011_01_monthly.pdf.
Kalnay, E., Kanamitsu, M., Kistler, R., Collins, W., Deaven, D., Gandin, L., Iredell, M., Saha, S., White, G., Woollen, J., Zhu, Y., Chelliah, M., Wang, J., Leetmaa, A., Reynolds, R., Jenne, R., Joseph, D., 1996. The NCEP/NCAR 40-year reanalysis project. Bull. Am. Meteorol. Soc. 77, 437–470.
Kato, K., Shin'ichi, M., Yamauchi, H., 2013. 2010–2011 Eruptive activity of Shinmoedake Volcano, Kyushu, Japan. Available at http://kcs.dvo.ru/ivs/slsecret/jkasp_2011/abstr/abs34.pdf.
Kienle, J., Shaw, G.E., 1979. Plume dynamics, thermal energy and long distance transport of vulcanian eruption clouds from Augustine volcano, Alaska. J. Volcanol. Geotherm. Res. 6, 139–164.
Kochi University, 2013. Weather Satellite Image Archive, GMS/GOES9/MTSAT Data Archive for Research and Education. Available at http://weather.is.kochi-u.ac.jp/archive-e.html.
Kozono, T., Ueda, H., Ozawa, T., Koyaguchi, T., Fujita, E., Tomiya, A., Suzuki, Y.J., 2013. Magma discharge variations during the 2011 eruptions of Shinmoe-dake volcano, Japan, revealed by geodetic and satellite observations. Bull. Volcanol. 75, 695. http://dx.doi.org/10.1007/s00445-013-0695-4.
Lacava, T., Marchese, F., Pergola, N., Tramutoli, V., Coviello, I., Faruolo, M., Paciello, R., Mazzeo, G., 2011. RSTVOLC implementation on MODIS data for monitoring of thermal volcanic activity. Special issue V3-LAVA project. Ann. Geophys. 54 (5), 1–7. http://dx.doi.org/10.4401/ag-5337.
Lin, Z., Jian, L., Cheng, L., Meng, W., 2011. Satellite remote sensing of volcanic ash cloud in complicated meteorological conditions. Sci. China Ser. D Earth Sci. 1–7. http://dx.doi.org/10.1007/s11430-011-4265-3.
Maeno, F., Nagai, M., Nakada, S., Burden, R., Engwell, S., Suzuki, Y., Kaneko, T., 2012. Constraining tephra dispersion and deposition from cyclic subplinian explosions at Shinmoedake volcano, Kyushu, Japan, 2012. Abst Japan Geoscience Union Meet SVC50-07.
Maki, M., Maesaka, T., Kozono, T., Nagai, N., Furukawa, R., Nakada, S., Koshida, T., Takenaka, H., 2012. Quantitative volcanic ash estimation by operational polarimetric weather radar. Available at http://cetemps.aquila.infn.it/istp/proceedings/Session_C_Aerosols_clouds_and_precipitation/Session_C_Wednesday_5_September_2012/SC_07_Maki.pdf.
Marchese, F., Filizzola, C., Genzano, N., Mazzeo, G., Pergola, N., Tramutoli, V., 2011a. Assessment and improvement of a Robust Satellite Technique (RST) for thermal monitoring of volcanoes. Remote Sens. Environ. 115 (6), 1556–1563.
Marchese, F., Filizzola, C., Mazzeo, G., Pergola, N., Sannazzaro, F., Tramutoli, V., 2011b. Assessment and validation in time domain of a Robust Satellite Technique (RSTASH) for ash cloud detection. GNH&R, Special issue on "Passive satellite techniques and ground-based investigations for volcanic activity monitoring. 1–16. http://dx.doi.org/10.1080/19475705.2011.564211.
Marchese, F., Lacava, T., Pergola, N., Hattori, K., Miraglia, E., Tramutoli, V., 2012. Inferring phases of thermal unrest at Mt. Asama (Japan) from infrared satellite observations. J. Volcanol. Geotherm. Res. 237, 10–18.
Mastin, L.G., Guffanti, M., Servranckx, R., Webley, P., Barsotti, S., Dean, K., Durant, A., Ewert, J.W., Neri, A., Rose, W.I., Schneider, D., Siebert, L., Stunder, B., Swanson, G., Tupper, A., Volentik, A., Waythomas, C.F., 2009. A multidisciplinary effort to assign realistic source parameters to models of volcanic ash-cloud transport and dispersion during eruptions. J. Volcanol. Geoth. Res. 186, 10–21. http://dx.doi.org/10.1016/j.jvolgeores.2009.01.008.
Miyabuchi, Y., Hanada, D., Niimi, H., Kobayashi, T., 2013. Stratigraphy, grain-size and component characteristics of the 2011 Shinmoedake eruption deposits, Kirishima Volcano, Japan. J. Volcanol. Geotherm. Res. 258, 31–46.
Mizota, C., Faure, K., 1998. Hydrothermal origin of smectite in volcanic ash. Clay Clay Miner. 46 (2), 178–182.
National Aeronautics and Space Administration (NASA), 2013a. Earth Observatory. Available at http://earthobservatory.nasa.gov/NaturalHazards/view.php?id=48945.
National Aeronautics and Space Administration (NASA), 2013b. Lidar browse images. Available at http://www-calipso.larc.nasa.gov/products/lidar/browse_images/production/.
Neal, C.A., McGimsey, R.G., Gardner, C.A., Harbin, M.L., Nye, C.J., 1994. Tephra-fall from 1992 eruptions of Crater Peak, Mount Spurr Volcano, Alaska: a preliminary report on distribution, stratigraphy and composition. U.S. Geol. Surv. Bull. 2139.
Oppenheimer, C., 1998. Volcanological applications of meteorological satellites. Int. J. Remote Sens. 10, 2829–2864.
Pavolonis, M.J., Wayne, F.F., Heidinger, A.K., Gallina, G.M., 2006. A daytime complement to the reverse absorption technique for improved automated detection of volcanic ash. J. Atmos. Ocean. Technol. 23, 1422–1444.
Pergola, N., Marchese, F., Tramutoli, V., 2004a. Automated detection of thermal features of active volcanoes by means of infrared AVHRR records. Remote Sens. Environ. 93, 311–327.
Pergola, N., Tramutoli, V., Marchese, F., Scaffidi, I., Lacava, T., 2004b. Improving volcanic ash cloud detection by a robust satellite technique. Remote Sens. Environ. 90, 1–22.
Picchiani, M., Chini, M., Corradini, S., Merucci, L., Sellitto, P., Del Frate, F., Stramondo, S., 2011. Volcanic ash detection and retrievals from MODIS data by means of Neural Networks. Atmos. Meas. Tech. 4, 2619–2631. http://dx.doi.org/10.5194/amt-4-2619-201.
Piscini, A., Corradini, S., Marchese, F., Merucci, L., Pergola, N., Tramutoli, V., 2011. Volcanic ash cloud detection from space: a comparison between the RSTASH technique and the water vapour corrected BTD procedure. GNH&R, Special Issue on "Passive satellite techniques and ground-based investigations for volcanic activity monitoring". 1–15. http://dx.doi.org/10.1080/19475705.2011.568069.
Prata, A.J., 1989. Observations of volcanic ash clouds in the 10–12 μm window using AVHRR/2 data. Int. J. Remote Sens. 10, 751–761.
Prata, A., Grant, I., 2001. Retrieval of microphysical and morphological properties of volcanic ash plumes from satellite data: application to Mt Ruapehu, New Zealand. Q. J. R. Meteorol. Soc. 127, 2153–2179. http://dx.doi.org/10.1256/smsqj.57614.
Richards, M.S., Ackerman, S.A., Pavolonis, M.J., Feltz, W.F., Tupper, A., 2006. Volcanic ash cloud heights using the MODIS CO_2-slicing algorithm. CIMSS. University of Wisconsin-Madison, Department of Atmospheric and Oceanic Sciences, Madison.
Rolph, G.D., 2013. Real-time Environmental Applications and Display sYstem (READY). Website (http://ready.arl.noaa.gov) NOAA Air Resources Laboratory, Silver Spring, MD.
Satellite Program Division (SPD), 2009. Switchover of meteorological mission. Plan for Switchover of Meteorological Mission from MTSAT-1R to MTSAT-2, Japan Meteorological Agency, 30 July 2009. (Available at http://mscweb.kishou.go.jp/notice/switch_over_e.htm).
Sawada, Y., 1987. Study on Analysis of Volcanic Eruptions Based on Eruption Cloud Image Data Obtained by the Geostationary Meteorological Satellite (GMS). Meteorology Research Institute (Japan), Tokyo (335 pp.).
Sawada, Y., 2002. Analysis of eruption cloud with Geostationary Meteorological Satellite imagery (Himarwari). J. Geogr. (Japan) 111, 374–394.
Settle, M., 1978. Volcanic eruption clouds and the thermal power output of explosive eruptions. J. Volcanol. Geotherm. Res. 3, 309–324.
Shimbori, T., Fukui, K., 2012. Time variation of the eruption cloud echo height from Shinmoe-dake Volcano in 2011 observed by Tanegashima and Fukuoka Weather Radars: Part II. Rep Coordinating Comm Prediction of Volcanic Eruption, 109 173–178.
Sparks, R.S.J., Bursik, M.I., Carey, S.N., Gilbert, J.S., Glaze, L.S., Sigurdsson, H., Woods, A.W., 1997. Volcanic Plumes. John Wiley, New York (574 pp.).
Stohl, A., Prata, A.J., Eckhardt, S., Clarisse, L., Durant, A., Henne, S., Kristiansen, N.I., Minikin, A., Schumann, U., Seibert, P., Stebel, K., Thomas, H.E., Thorsteinsson, T., Tørseth, K., Weinzierl, B., 2011. Determination of time- and height-resolved volcanic ash emissions and their use for quantitative ash dispersion modeling: the 2010 Eyjafjallajökull eruption. Atmos. Chem. Phys. 11, 4333–4351. http://dx.doi.org/10.5194/acp-11-4333-2011.
Support to Aviation Control Service (SACS). Available at http://sacs.aeronomie.be/.
Suzuki, T., 1983. A theoretical model for dispersion of tephra. In: Shimozuru, D., Yokoyama, I. (Eds.), Arc Volcanism: Physics and Tectonics. Terra Scientific Publishing Company (Terrapub), Tokyo, pp. 95–113.
Tokyo VAAC (Volcanic Ash Advisory Center) — Japan Meteorological Agency, Volcanic Ash Advisory, Archive, 2013. Volcanic ash advisories (2011). Date time: 10:20 UTC 26 Jan 2011, Volcano: Kirishimayama, Area: Japan Advisory Number: 2011/10. Available at http://ds.data.jma.go.jp/svd/vaac/data/Archives/2011_vaac_list.html.
Tramutoli, V., 1998. Robust AVHRR Techniques (RAT) for environmental monitoring theory and applications. In: Cecchi, Giovanna, Zilioli, Eugenio (Eds.), Earth Surface Remote Sensing II. SPIE, 3496, pp. 101–113.
Tramutoli, V., 2007. Robust Satellite Techniques (RST) for natural and environmental hazards monitoring and mitigation: theory and applications. Proceedings of Multitemp. http://dx.doi.org/10.1109/MULTITEMP.2007.4293057.
Tsunomura, S., 2011. Current status and future plan of Japanese Meteorological Satellite Program. The Second Asia/Oceania Meteorological Satellite Users' Conference 6–9 December 2011, Tokyo, Abstracts Brochure.
Tupper, A., Carn, S., Davey, J., Kamada, Y., Potts, R., Prata, F., Tokuno, M., 2004. An evaluation of volcanic cloud detection techniques during recent significant eruptions in the western 'Ring of Fire'. Remote Sens. Environ. 91, 27–46.

Tupper, A., Textor, C., Herzog, M., Graf, H.F., Richards, M.S., 2009. Tall clouds from small eruptions: the sensitivity of eruption height and fine ash content to tropospheric instability. Nat. Hazards 51, 375–401.

Walker, G.P.L., 1980. The Taupo pumice: product of the most powerful known (ultraplinian) eruption. J. Volcanol. Geotherm. Res. 8 (1), 69–94. http://dx.doi.org/10.1016/0377-0273(80)90008-6.

Webley, P.W., Mastin, L.G., 2009. Improved prediction and tracking of volcanic ash clouds. In: Mastin, Larry, Webley, Peter (Eds.), J. Volcanol. Geotherm. Res. Special Issue on Volcanic Ash Clouds. http://dx.doi.org/10.1016/j.jvolgeores.2008.10.022.

Webley, P.W., Lopez, T.M., Ekstrand, A.L., Dean, K.G., Rinkleff, P., Dehn, J., Cahill, C.F., Wessels, R.L., Bailey, J.E., Izbekov, P., Worden, A., 2012. Remote observations of eruptive clouds and surface thermal activity during the 2009 eruption of Redoubt Volcano. J. Volcanol. Geotherm. Res. http://dx.doi.org/10.1016/j.jvolgeores.2012.06.023.

Wen, S., Rose, W.I., 1994. Retrieval of sizes and total masses of particles in volcanic clouds using AVHRR bands 4 and 5. J. Geophys. Res. Atmospheres (1984–2012) 99 (D3), 5421–5431.

Wilson, L., Sparks, R.S.J., Huang, T.C., Watkins, N.D., 1978. The control of volcanic column heights by eruption energetics and dynamics. J. Geophys. Res. 83 (B4), 1829–1836.

Winker, D.M., Hunt, W.H., Hostetler, C.A., 2004. Status and performance of the CALIOP Lidar. Proc. SPIE Int. Soc. Opt. Eng. 5575, 8–15.

Winker, D.M., Hunt, W.H., McGill, M.J., 2007. Initial performance assessment of CALIOP. Geophys. Res. Lett. 34, L19803. http://dx.doi.org/10.1029/2007GL030135.

Winker, D., Vaughan, M., Omar, A., Hu, Y., Powell, K., Liu, Z., Hunt, W., Young, S., 2009. Overview of the CALIPSO mission and CALIOP data processing algorithm. J. Atmos. Ocean. Technol. 26, 2310–2323.

Wright, R., Flynn, L.P., Garbeil, H., Harris, A.J.L., Pilger, E., 2002. Automated volcanic eruption detection using MODIS. Remote Sens. Environ. 82, 135–155.

Yu, T., Rose, W.I., Prata, A., 2001. Atmospheric correction for satellite-based volcanic ash mapping and retrievals using “split window” IR data from GOES and AVHRR. J. Geophys. Res. 107, 20.

Zakšek, K., Hort, M., Zaletelj, J., Langmann, B., 2013. Monitoring volcanic ash cloud top height through simultaneous retrieval of optical data from polar orbiting and geostationary satellites. Atmos. Chem. Phys. 13, 2589–2606.